Dyslipidemia in the Young: From Genotype to Treatment

Balder, Jan-Willem

Stap1 knockout mice

Studying the Role of STAP1 in Cholesterol Metabolism: Characterization of *Stap1* Knockout Mice

J.W. Balder[1,2], J.C. Wolters[1], M. Smit[1], N.J. Kloosterhuis[1], H. Douna[3], J. Kuiper[3], J.H.M. Levels[4], A.J.A. van de Sluis[1], J.A. Kuivenhoven[1*]

1. Department of Pediatrics, Section Molecular Genetics, University Medical Center Groningen, University of Groningen, Groningen, the Netherlands.
2. Department of Vascular Medicine, University Medical Center Groningen, University of Groningen, Groningen, the Netherlands.
3. Division of Biotherapeutics, LACDR, Leiden University, Leiden, the Netherlands.
4. Department of Vascular Medicine, Academic Medical Center, University of Amsterdam, Amsterdam, the Netherlands.

*Corresponding author: j.a.kuivenhoven@umcg.nl

8

In preparation

Abstract

Aim

Recently, mutations in signal transducing adaptor protein 1 (*STAP1*) were reported to be associated with familial hypercholesterolemia in man. This gene is mainly expressed in immune cells such as B-lymphocytes, but how STAP1 may control cholesterol homeostasis is unclear. Here, we generated and characterized whole body *Stap1* knockout (*Stap1*$^{-/-}$) mice to unravel the role of STAP1 in cholesterol homeostasis.

Methods

CRISPR/Cas9 was used to generate two different *Stap1* knockout mouse lines. Lack of expression of STAP1 was shown at protein level. Mice (n = 96) were studied on chow and on a high-fat-high-cholesterol (0.25% cholesterol; HFC) diet for four weeks. Measurements included plasma lipids, lipoprotein profiling, liver histology, hepatic lipid levels and FACS analyses of immune cells.

Results

Heterozygote and homozygote mice were born without overt phenotype and in expected Mendelian ratios. We did not observe differences in plasma lipids between *Stap1*$^{-/-}$ mice and wild-type littermates on chow, nor after feeding a HFC diet for four weeks. Unexpectedly, *Stap1*$^{-/-}$ males fed a HFC diet, gained significantly less weight, (29% *vs.* 38% increase; $p < 0.05$). In females, the difference in weight gain was not significant (15% *vs.* 32% increase). In both genders, *Stap1*$^{-/-}$ mice exhibited a marked macrovesicular steatosis *vs.* microvesicular steatosis in wild-type littermates. No differences in liver lipid levels were noted.

Conclusions

A complete loss of STAP1 in mice does not cause changes in plasma lipid metabolism. This deviates from the assumption that STAP1 mediates plasma cholesterol levels in humans. The discrepancy could be due to species differences but it is also possible that the identified human *STAP1* mutations are gain-of-function mutations. The data thus far do not support a role for STAP1 in murine lipid metabolism but further studies into a possible interaction between the immune system and lipid metabolism are warranted.

Introduction

Cardiovascular disease (CVD) is the most common cause of death worldwide.[1] Increased plasma levels of cholesterol, especially low-density lipoprotein cholesterol (LDL-c), are an important risk factor for CVD. Mutations in the genes encoding for the LDL receptor (*LDLR*), apolipoprotein B (*APOB*) and proprotein convertase subtilisin/kexin type 9 (*PCSK9*) can cause reduced clearance of LDL from blood.[177] The disease caused by these genetic defects is known as familial hypercholesterolemia (FH; OMIM#143890). FH is one of the most common monogenetic diseases with almost 1 in 200 individuals expected to be affected. However, in a substantial proportion of patients with clinical FH, the molecular etiology of hypercholesterolemia remains unknown.[202] Genome-wide association studies (GWAS) have provided many clues towards which (additional) genetic loci may be involved in determining plasma LDL-c levels. The respective genetic information has improved the study of polygenic origins of FH (defined by an accumulation of multiple common variants with small effect sizes on LDL-c)[15] and respective assessment tools have been added to FH diagnosis screening platforms.[191] Molecular studies following GWAS have improved our insight in LDL metabolism, but such investigations are scarce.[203] In addition, family studies keep being employed to increase our understanding of LDL metabolism.[204] After the finding of *PCSK9* through linkage analysis,[34] another study showed that missense mutations in *STAP1*, encoding for signal transducing adaptor protein 1, were associated with hypercholesterolemia. After the initial finding in one family, sequencing of *STAP1* in 400 unrelated index patients with unknown causes of FH, led to the identification of additional *STAP1* mutations.[205] Another research group found a novel variant in *STAP1* in a small family with premature CVD and increased LDL-c levels.[206] Together these studies suggest a role of STAP1 in human LDL metabolism.

Studies with human tissues and cells have shown that the expression of *STAP1* is largely restricted to (EBV transformed) lymphocytes, kidney, small intestine and spleen (GTEx). In mice, *Stap1* has been reported to be highly expressed in hematopoietic stem cells[207], microglia, bone marrow, spleen and thymus.[208] The STAP1 protein consists of 295 amino acids and has a pleckstrin homology domain and an Src homology domain 2. The Src homology domain 2 is also present in receptor tyrosine kinases, which are high-affinity receptors for growth factors, cytokines and hormones.[207]

Taken together, the finding that STAP1 may play a role in lipid metabolism is intriguing when considering its suggested role in the immune system. In this context, we have generated and characterized a whole body *Stap1* knockout mouse model to explore the role of STAP1 in the control of plasma cholesterol levels.

Material and methods

Generation of Stap1$^{-/-}$ mice using CRISPR/Cas9

The protocol used to design and validate the effectiveness of sgRNA *in vitro* has been described previously.[209] In short, two sgRNAs, targeting exon 3 of *Stap1*, were designed (crispr.mit.edu). The top and bottom strands were annealed and phosphorylated. The phosphorylated and annealed sgRNAs were diluted (1:200) and cloned into the pX459 vector and ligated with T7 DNA ligase. After ligation, a PlasmidSafe exonuclease reaction was performed to digest any residual linearized DNA. After the transformation into DH5α, the clones containing sgRNA were validated by sequencing analysis.

Neuro2A cells were seeded in 6-well plates at a density of 300,000 cells per well, and reached a confluency of 70 – 80% after 24 hours. In 95.2 µl serum free DMEM-glutamax, 4.8 µl Fugene6 was added and incubated for 5 min at room temperature (RT). Subsequently, 1 µg pX459 containing the sgRNA was added and incubated for 15 min at RT. After 24 and 48 hours, the medium was changed with medium containing 5 µg/ml puromycin, after which DNA was isolated. The DNA was dissolved in 1x TE buffer and incubated for 10 min at 65°C and rotated over night at RT to dissolve.

A surveyor PCR was performed using *Stap1* specific primers (Fw primer 5'-TACTGAGCACGGCATGTGAC-'3; Rev primer 5'-GCCTGAGTTCCAGTCCTGAC-'3) using the following conditions: 5 min 95°C; 30 cycles of 30 sec 95°C, 30 sec 60°C, 30 sec 72°C; 2 min 72°C, hold 10°C. After confirming a specific fragment using a 1% wt/vol agarose gel containing midori green, the remaining PCR product was purified using a QIAQuick PCR purification kit according to the manufacturer's instructions. A DNA heteroduplex was formed. A surveyor nuclease S digestion was performed for 30 min at 42°C according to the manufacturer's instructions (Transgenomic). Ten µl product was analyzed on a 2% wt/vol agarose gel containing midori-green and the indel percentage was calculated. A PCR reaction was performed to add the T7 promoter to the Cas9 coding region (Fw primer 5'-TAATACGACTCACTATAGGGAGAATGACTATAAGGACCACGAC-'3; and Rev primer 5'-GCGAGCTCTAGGAATTCTTAC-'3) and to the sgRNA coding region (Fw primer 5'-TTAATACGACTCACTATAGGATAGACCTCGTGTGCCTTAC-'3; and Rev primer 5'- TTTAAAAGCACCGACTCGGTGCC-'3). After confirming a specific fragment using a 1% wt/vol agarose gel containing midori green, the remaining PCR product was purified using a QIAQuick PCR purification kit according to the manufacturer's instructions. The PCR product was ligated in pZero blunt and transformed in DH5α cells. A few colonies were picked for Sanger sequencing. Plasmids containing the correct insert were digested and isolated from gel and purified using a standard ethanol precipitation. *Stap1* sgRNA was generated using the MEGAshortscript kit (Ambion) using 125 nM input, while Cas9 RNA was generated using the mMESSAGE mMACHINE T7 ULTRA kit (Ambion) using 125 nM input. sgRNA was purified using the MEGAclear kit (Ambion) and eluted in RNAse free water.

Zygote injections

I29 FVB females were super ovulated by injection with 5 IU Folligonan (0.2 ml intraperitoneal) and 48 h later with 5 IU Chorulon (0.2 ml intraperitoneal). The next day, zygotes were isolated from the infundibulum and injected with 100 ng/µl Cas9 RNA + 50 ng/µl sgRNA *Stap1*. Injected zygotes were incubated over night at 37ºC and transferred to the infundibulum of pseudopregnant females.

Genotyping

To determine the presence of mutations in *Stap1* of the offspring upon Cas9 mRNA and sgRNA injection in zygotes, we isolated genomic DNA from small ear cuts of the mice. The ear-pieces were incubated in 500 µl 1x SE supplemented with 50 µl 10% SDS and 5 µl proteinase k (20 mg/ml) at 55ºC until dissolved. To each tube, 222 µl 6M saturated NaCl and 777 µl chloroform was added. After centrifugation for 10 min at 12,000 g RT, the upper phase was transferred to a new tube and diluted 1:1 with isopropanol. Subsequently, DNA was centrifuged for 10 min at 12,000 g RT. The pellet was air-dried and dissolved in distilled RNAse/DNAse free water (Gibco) before measuring the concentration using Nanodrop. A surveyor PCR was performed as described above. The F1 offspring was Sanger sequenced and analyzed for mutations.

Stap1$^{+/-}$ *x Stap1*$^{+/-}$ (non-littermates) breeding pairs were used to get *Stap1*$^{-/-}$ pups and offspring were genotyped. DNA was isolated from the ears by adding a solution of 17.8 µl mQ, 2.0 µl buffer Gold and 0.2 µl prepGEM. The sample was heated for 15 minutes at 75ºC and subsequently 95ºC for 5 minutes. A surveyor PCR was performed as described before. After confirming a specific fragment using a 1% wt/vol agarose gel containing midori green, the remaining PCR product was cut overnight with BglI (New England Biolabs) at 37ºC. Thereafter, loading dye was added in a 1:1 ratio, and the product was loaded on a 1% wt/vol agarose gel. The restriction enzyme will cut a specific nucleotide sequence, only present on alleles without mutation. Therefore, the length and the number of PCR fragments determines the genotype.

Animals

This animal study was approved by the Institutional Animal Care and Use Committee, University of Groningen (Groningen, the Netherlands). We characterized *Stap1*$^{-/-}$, *Stap1*$^{+/-}$, and *Stap1* wild-type mice with FVB background for two different *Stap1* mutated mouse lines, males and females separately (n = 8 per group; in total 96 mice). All mice were group-housed (littermates only). Until ~13 weeks of age all mice were fed a standard rodent chow diet (RMH-B, AB Diets, the Netherlands) ad libitum. Before termination, all mice received a high-fat-high-cholesterol (HFC, cholesterol 0.25%) diet ad libitum, for four weeks, until ~17 weeks

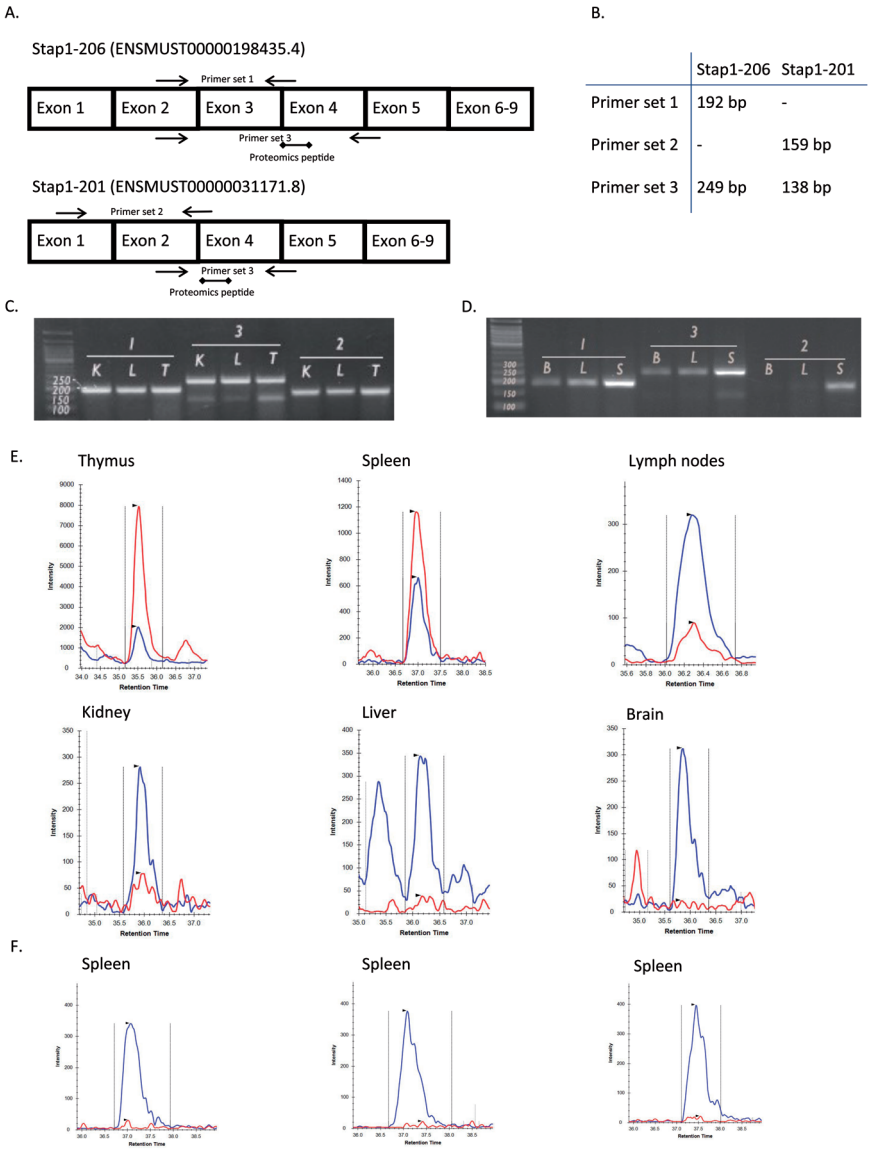

Figure 1. *Stap1* RNA and protein expression.

Figure 1A shows the two protein-coding transcripts of *Stap1* in mice. The targeting peptide for proteomics is in exon 4. We designed three transcript-specific primers. Primer 1 targets transcript *Stap1*-206, primer 2 targets *Stap1*-201, and primer 3 targets both transcripts. The expected PCR products are present in Figure 1B. Figure 1C shows the RNA expression of *Stap1* transcripts in the kidney (K), lymph nodes (L) and thymus (T), and Figure 1D shows the RNA expression of brain (B), liver (L) and spleen (S). Figure 1E shows the presence of STAP1 protein in different organ tissues from mice using targeted proteomics (blue is spiked standard and red is endogenous peptide). Figure 1F shows the absence of STAP1 protein, measured using targeted proteomics in homogenized spleen tissues of three Stap1$^{-/-}$ mice.

of age. Blood was taken through orbital punctures, after a 4-h morning fasting period, at ~13 weeks of age (just prior to the start of HFC-diet intervention), and at ~15 weeks of age. At termination blood was drawn by heart puncture. Plasma was collected after centrifugation at 3,000 rpm for 10 min at 4°C. At termination, tissues for mRNA and protein expression were snap frozen in liquid nitrogen and stored at -80°C.

Harvesting of organs

To study *Stap1* expression, we isolated RNA and proteins from harvested tissues (thymus, lymph nodes, spleen, liver, brain, and kidney) of three *Stap1*$^{-/-}$, and three *Stap1* wild-type mice of our experiment. After termination, tissues were isolated and snap-frozen in liquid nitrogen, and stored at -80°C until later use.

RNA isolation and cDNA synthesis. Fifty mg of harvested tissue was homogenized with 1 ml QIAzol Lysis (Qiagen). Chloroform extraction was used to isolate RNA. Isopropanol-precipitated and ethanol-washed RNA pellets were dissolved in 25 µl distilled RNAse/DNAse free water (Gibco). The RNA quantity and quality was measured with Nanodrop. cDNA was synthesized using ~2.0 µg RNA with the Transcriptor Universal cDNA Master, according to the manufacturer's instructions (Roche).

Protein lysates. Hundred mg of tissue was added to 1 ml of homogenization buffer. Fifty ml of homogenization buffer consisted of 48.45 ml 0.1% NP40 buffer (0.4M NaCl), 1 tablet protease inhibitor (Roche), 0.5 ml phosphate inhibitors 2 and 3 (Sigma-Aldrich), 50 µl 1M DTT and 500 µl NaOV.

Liver histology

After termination, complete livers were isolated, and the right hepatic lobe was fixed in formaline, embedded in paraffin, and cut into 4 µm sections. Due to the large design of our study, we decided to perform histopathological examination for only part of the mice. We selected all *Stap1* wild-type, and *Stap1*$^{-/-}$ mice from both genders for one mutation line (32 in total). For porphyrin measurements, liver sections were stained with hematoxylin-eosin and analyzed using ImageJ software. Slides were examined unbiased for the presence of histopathological lesions.

mRNA analyses

Stap1 has two protein coding transcripts, i.e. *Stap1*-206 (ENSMUST00000198435.4) and *Stap1*-201 (ENSMUST00000031171.8). The latter transcript lacks exon 3. Three primers were manually designed to investigate the transcript-specific RNA expression of *Stap1* (see Figure 1A and 1B). The first primer (Fw primer 5'-AACACTATTGGACGGAGCTG-'3; and Rev primer 5'-GTGTTTTCTGTCTTCACATGC'3) was specific for transcript *Stap1*-206 the second primer (Fw primer 5'-AGGAAAGACTGAAGATCACTG-'3; and Rev primer 5'-CTGTGTTTTCT

GTGATTGTGC-'3) was specific for transcript *Stap1*-201, whereas the third primer (Fw primer 5'-AACACTATTGGACGGAGCTG-'3; and Rev primer 5'-CTGAGGAACTGTCAACTCTGT-'3) targeted both transcripts. However, because transcript *Stap1*-201 misses exon 3, a difference of 111 basepairs can be detected. A PCR was performed using the following conditions: 5 min 95°C; 30 cycles of 30 sec 95°C, 30 sec 60°C, 30 sec 72°C; 2 min 72°C, hold 10°C. Thereafter, 20 µl product was analyzed on a 2.5% wt/vol agarose gel containing midori-green.

Protein analyses using mass spectrometry

Isotopically labeled standards were ordered from Polyquant (13C-labeled lysines and arginines) in the form of synthetic proteins consisting of peptide concatemers, designed to detect proteins of interest, including STAP1. For this peptide the optimal precursor charge and transitions are known. Homogenized tissues (50 µg of total protein) were resuspended in NuPAGE LDL loading buffer (Thermo Scientific) plus 0.05 to 0.10 ng QconCat per µg of total protein. After reduction with 10 mM dithiothreitol and alkylation with 55 mM iodoacetamide, proteins were subjected to in-gel tryptic digestion (1:100 g/g). Two µl was injected and loaded onto a trap column (µ-Precolumn cartridge, Acclaim PepMap100 C18, 5 µm, 100 A, Dionex). The STAP1 peptide (TENTESGEEWR) was targeted and analyzed by a triple quadrupole mass spectrometer equipped with a nano-electrospray ion source (TSQ Vantage, Thermo Scientific). The chromatographic separation (gradient 110 min) of the peptides was performed by liquid chromatography on a nano-UHPLC system (Ultimate UHPLC focused, Dionex).

The mass spectrometer traces were manually curated using the Skyline software prior to integration of the peak areas for quantification. The sum of all transition peak areas for the endogenous peptides and isotopically labeled QconCAT-peptide standards was used to calculate the ratio between the endogenous and standard peptides. The concentrations of the endogenous peptides were calculated from the known concentrations of the standards and expressed in fmol/µg of total protein. If the endogenous peptide was not detected in the samples, but the isotopically labeled standards were, the peptide was considered to be absent.

Lipid measurements

Total cholesterol levels were measured using colorimetric assay (11489232, Roche Molecular, Biochemicals) with cholesterol standard FS (DiaSys Diagnostic Systems) as a reference. Triglyceride levels were measured using Trig/GB kit (1187771, Roche Molecular, Biochemicals) with Roche Precimat Glycerol standard (16658800, Roche Molecular Biochemicals) as a reference.

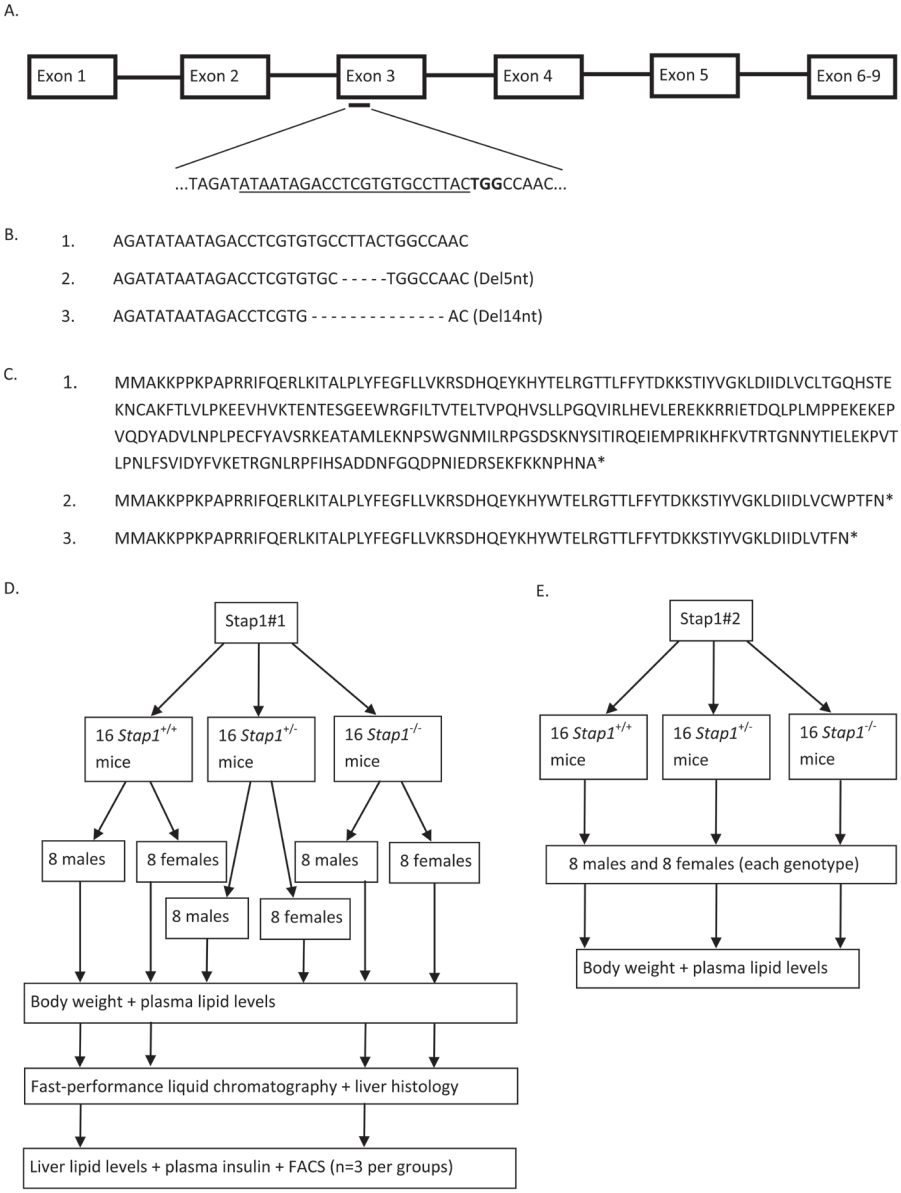

Figure 2. Generation of whole body *Stap1*$^{-/-}$ mice and outline of study protocol.
Figure 2A shows the sequence of the sgRNA (underlined sequence) used for targeting exon 3 of the murine *Stap1* gene. Part of the DNA sequence of *Stap1* wild-type is shown in the first row of Figure 2B. Row 2 and 3 show the DNA sequence of two mouse lines with two different indel mutations. The corresponding amino acid sequences are presented in Figure 2C. Both deletions result in a premature stop codon (*). Figure 2D shows the analyses performed in del5nt mouse strain (Stap1#1). Figure 2E shows the analyses performed in del14nt mouse strain (Stap1#2).

Fast-performance liquid chromatography

Cholesterol fractions in the main lipoprotein classes (VLDL, LDL and HDL) were determined using FPLC for each *Stap1* wild-type and *Stap1*$^{-/-}$ mouse separately. The system contained a PU-980 ternary pump with an LG-980-02 linear degasser, FP-920 fluorescence and UV-975 UV/VIS detectors (Jasco, Tokyo, Japan). An extra PU-2080i Plus pump (Jasco, Tokyo Japan) was used for in-line triglyceride enzymatic reagent or cholesterol PAP (Roche, Basel, Switzerland) addition at a flowrate of 0.1 ml/min. Separation of plasma lipoproteins was performed with a Superose 6 HR 10/30 column (GE Healthcare Hoevelaken, the Netherlands) using TBS pH 7.4, as eluent at a flow rate of 0.31 ml/min. ChromNav chromatographic software, version 1.0 (Jasco, Tokyo, Japan), was used for quantitative analysis of the chromatograms.

Flow cytometry analysis

Using harvested organs from three male *Stap1* wild-type and three male *Stap1*$^{-/-}$ mice FACS analysis was performed after termination. Heart lymph nodes, mesenteric lymph nodes, spleen and plasma were harvested directly after the termination. Primary cells were isolated with the use of Cell Strainers (Greiner bio-one easystrainer 70 µm sterile, no 542070) following manufacturer's instructions. Two hundred µl blood was mixed with 500 µl ACK lysing buffer (Gibco). After waiting for 2 minutes, 500 µl RPMI 1640 medium (Gibco) was added and centrifuged for 5 minutes (1500 rpm). The pellet was dissolved in 200 µl RPMI 16040 medium (Gibco). Different selection/sorting methods were performed to identify the different immune subpopulations in the tissues (see Supplementary Table 1 – 4).

Statistical analysis

The figures were made using Sigmaplot (Systat Software, San Jose, CA, USA). Statistics were performed using PASW Statistics (Version 23, IBM, Armonk, NY, USA). Data are presented as mean and standard deviation. The means of two groups were compared using Student's *t*-test. The means of three groups were compared using one-way ANOVA with Tukey post hoc analysis. To determine differences of lipid levels and weight during the experiment between genotype a Two-Way Mixed ANOVA was used.

Results

Stap1 is not ubiquitously expressed in mice

Unlike humans, mice have two isoforms of *Stap1*, namely transcript *Stap1*-206 (ENSMUST00000198435.4) and *Stap1*-201 (ENSMUST00000031171.8). The main difference between these two transcripts is the absence of exon 3 in *Stap1*-201 (Figure 1A). Since in humans only one isoform has been identified and three out of five *STAP1* mutations in FH families are located in exon 3,[205, 206] we first investigated the expression of the two transcript

variants in different tissues of wild-type mice. Three different primer sets (Figure 1A) were used to detect: 1) *Stap1*-206; 2) *Stap1*-201; or 3) both *Stap1*-206 and *Stap1*-201. The expected length of the PCR products is given in Figure 1B. Due to the absence of exon 3 in *Stap1*-201 the PCR product, generated by primer set 3, of this transcript is expected to be 111 bp smaller. Figures 1C and 1D show that *Stap1*-206 and *Stap1*-201 transcripts are present in the kidney (K), lymph nodes (L), thymus (T), and spleen (S). *Stap1*-201 is however not present in the brain (B) and the liver (L). Importantly, the RT-PCR results obtained through using primer set 3 suggest that *Stap1*-201 expression is much less abundant (despite the also smaller size of the respective PCR product) compared to *Stap1*-206 (see Figure 1C and 1D). These results indicate that in wild-type mice, the *Stap1*-201 variant is unlikely to play a role and that targeting exon 3 of murine *Stap1* will likely result in a loss-of-function mutation.

Generation of *Stap1* knockout mice

Targeting exon 3 of *Stap1* (Figure 2A) resulted in two different mutations that were initially studied in two different mouse lines. The first line (Stap1#1) carries a 5-base pair deletion, and the second line (Stap1#2) a 14-base pair deletion (Figure 2B). Both deletions result into a premature stop codon (Figure 2C). Figures 2D and 2E provide an overview of the number of mice studied and the different analyses that were performed. Mice were born in the expected Mendelian ratios without an overt phenotype.

STAP1 protein expression and functional consequences of *Stap1* mutations

Our studies with three commercially available antibodies against STAP1 provided inconsistent results which led us to the development of a targeted proteomics strategy to determine the protein levels of STAP1 in different mouse tissues. The peptide was analogue to a region encoded by exon 4 of *Stap1*. In wild-type mice (Stap1#1), STAP1 was detected at high abundance in thymus and spleen, at low abundance in the lymph nodes and kidney, and was not detected in liver and brain homogenates (see Figure 1E, red is endogenous peptide and blue spiked standard). Importantly, protein expression of STAP1 was not seen in spleen homogenates of three *Stap1*$^{-/-}$ mice (Figure 1F), indicating that a 5-base pairs deletion in *Stap1* exon 3 results in a loss-of-function mutation.

STAP1 does not control plasma lipids in mice

Heterozygosity for *STAP1* mutations in humans is correlated with familial hypercholesterolemia. However, at 13 weeks of age on chow diet, male and female *Stap1*$^{-/-}$ and their wild-type littermates showed similar total cholesterol levels (Figure 3A), as well after a four-week HFC-diet intervention at 17 weeks of age (Figure 3B). In addition, triglyceride levels were not

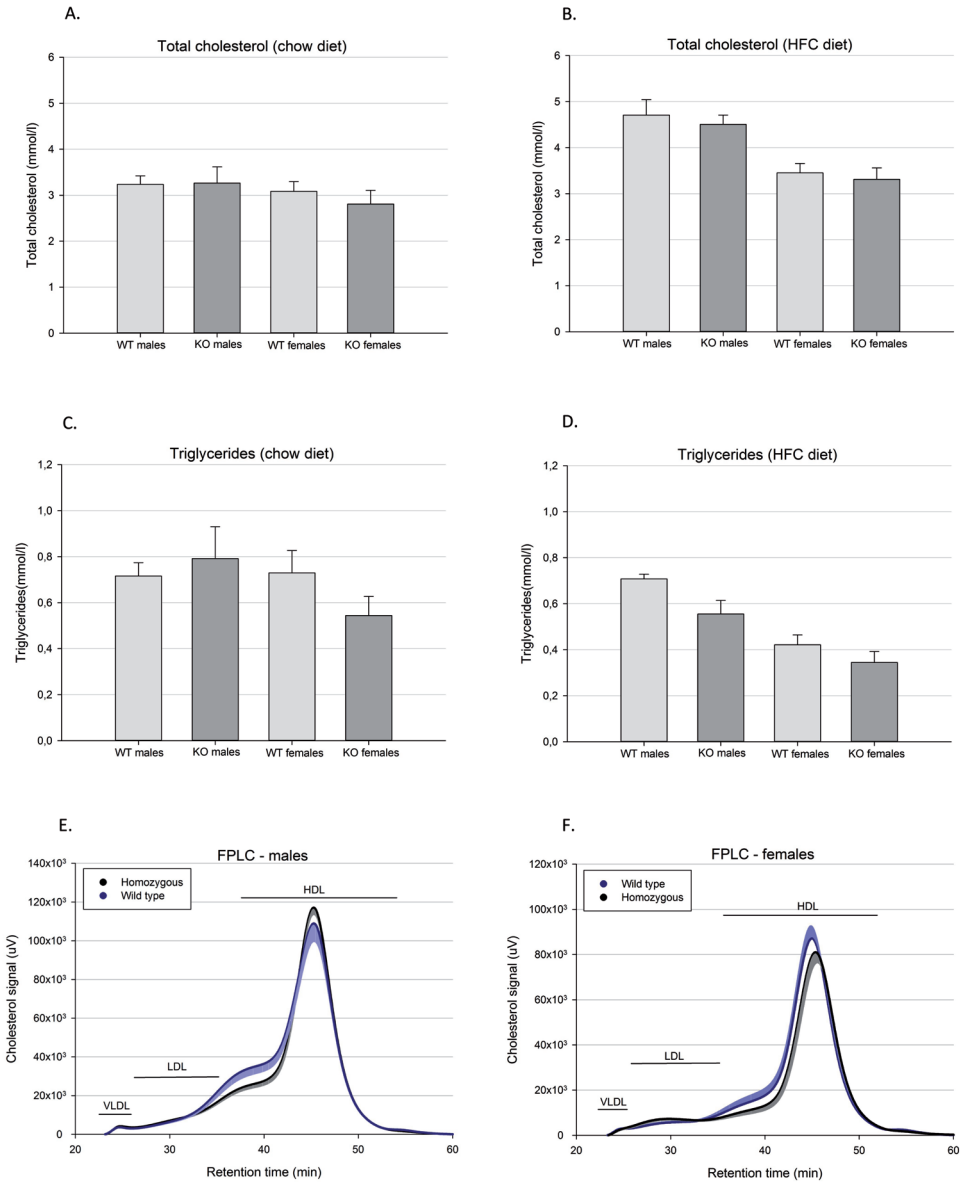

Figure 3. Lipid characterization. Data are presented as mean and standard error.
Figure 3A shows the mean plasma total cholesterol levels of mice ~13 weeks of age on chow diet. No differences between *Stap1* wild-type and knockout are present, nor after a four-week high-fat-high-cholesterol (HFC) diet (Figure 3B) when the mice are ~17 weeks of age. Figure 3C and 3D show the plasma triglyceride levels. Figure 3E and 3F show the mean (dark) and standard error (light) lipoprotein fractions separated by FPLC (measured individually) of plasma obtained during termination.

different amongst groups at 13 weeks of age, neither after a four-week HFC-diet intervention (Figure 3C and 3D). Plasma lipid levels for STAP1#2 are presented in Supplementary Figure 1A – D.

Using plasma obtained at termination, we also ran individual lipoprotein profiles of *Stap1*$^{-/-}$ mice and wild-type littermates using size exclusion chromatography. As expected in mice, most of the cholesterol was present in HDL fraction, but the profiles do not differ significantly at any timepoint between genotypes (Figure 3E and 3F).

Decreased body weight gain and markedly different liver histology

During the HFC diet intervention, *Stap1*$^{-/-}$ males and females gained substantially less body weight compared to wild-type littermates. Heterozygote male mice showed an intermediate phenotype. At the end of the experiment, a difference of ±7 and ±6 grams of body weight was observed in *Stap1*$^{-/-}$ males and females, respectively, in comparison to wild-type littermates (Figure 4A and 4B). Post-hoc analysis of Two-Way Mixed ANOVA shows that the difference between *Stap1*$^{-/-}$ and wild-type littermates is significantly different in males from week 15 and onwards ($p < 0.05$). In the females, however, the observed difference in weight is not significantly different. Supplementary Figure 1D and 1E show the change in weight during the HFC diet of STAP1#2 mice.

The difference in weight did not result in dissimilarities in liver weight and liver to body weight ratios amongst genotypes (Figure 4C and 4D). Hepatic lipid content (including total cholesterol, free cholesterol, cholesterol esters, and triglycerides) was similar in *Stap1*$^{-/-}$ and *Stap1* wild-type males (Figure 4E). In addition, histological analysis of the liver of wild-type and *Stap1*$^{-/-}$ mice reported no difference in steatosis, inflammation and NAS (Figure 4F). Interestingly, the liver steatosis of *Stap1* wild-type mice of both genders was mainly of a microvesicular type versus a macrovesicular type in the *Stap1*$^{-/-}$ mice. Representative photomicrographs of H&E-stained liver samples are shown for male wild-type (Figure 4G), male *Stap1*$^{-/-}$ (Figure 4H), female wild-type (Figure 4I), and female *Stap1*$^{-/-}$ (Figure 4J).

In conclusion, ablation of *Stap1* in mice deteriorates diet-induced weight gain. In STAP1#1 males the difference in weight gain was statistically different. A trend towards lower weight gain was furthermore observed in STAP1#2 knockout males, STAP1#1 and STAP1#2 knockout females. Furthermore, upon a HFC diet intervention, *Stap1*$^{-/-}$ mice displayed a macrovesicular liver steatosis while *Stap1* wild-type mice mainly showed microvesicular liver steatosis.

Ablation of STAP1 in mice does minimally effect immune cells

In view of the anticipated role of STAP1 in the immune system we performed an initial FACS analysis on three *Stap1*$^{-/-}$ males and wild-type littermates (see Figure 1A). Supplementary Figure 2A shows that there are no differences between the number of B cells present in spleen, heart lymph nodes (HLN), mesenteric lymph nodes (MLN) and blood. Supplementary

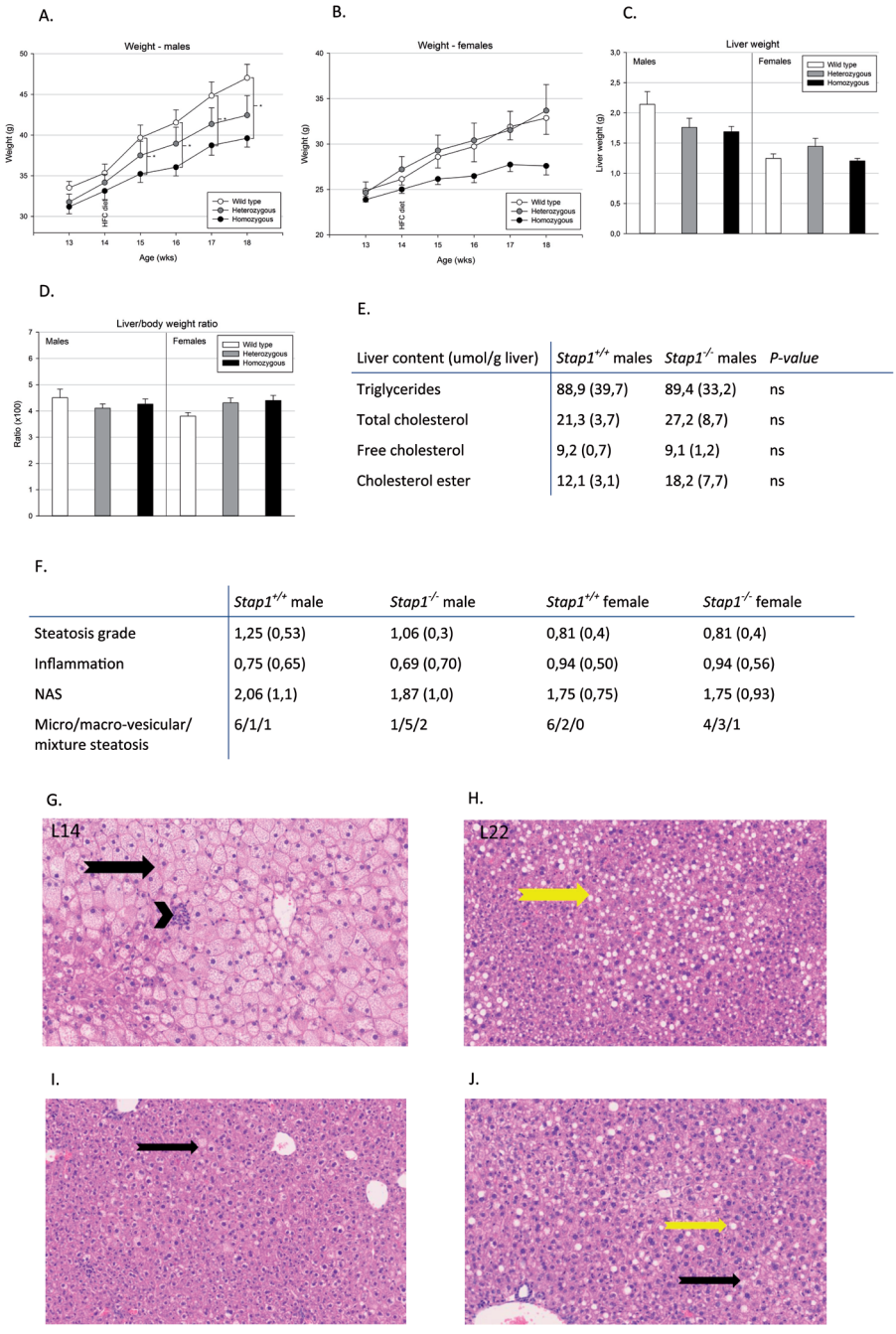

E.

Liver content (umol/g liver)	*Stap1*$^{+/+}$ males	*Stap1*$^{-/-}$ males	*P-value*
Triglycerides	88,9 (39,7)	89,4 (33,2)	ns
Total cholesterol	21,3 (3,7)	27,2 (8,7)	ns
Free cholesterol	9,2 (0,7)	9,1 (1,2)	ns
Cholesterol ester	12,1 (3,1)	18,2 (7,7)	ns

F.

	Stap1$^{+/+}$ male	*Stap1*$^{-/-}$ male	*Stap1*$^{+/+}$ female	*Stap1*$^{-/-}$ female
Steatosis grade	1,25 (0,53)	1,06 (0,3)	0,81 (0,4)	0,81 (0,4)
Inflammation	0,75 (0,65)	0,69 (0,70)	0,94 (0,50)	0,94 (0,56)
NAS	2,06 (1,1)	1,87 (1,0)	1,75 (0,75)	1,75 (0,93)
Micro/macro-vesicular/ mixture steatosis	6/1/1	1/5/2	6/2/0	4/3/1

Figure 4. Metabolic characterization.

Figure 4A and 4B show the progression of body weight during our experiment. Stap1$^{-/-}$ males gained significantly less weight during the experiment. A similar observation was present in females, but did not reach statistical significance. No differences in liver weight and liver/body weight ratio were present between genotypes (Figure 4C and 4D). No differences were present in the lipid liver content (Figure 4E). Figure 4F shows the mean (SD) of H&E-stained liver histopathological findings. Steatosis (amount of lipid accumulation) was scored as grade 0 (< 5%), 1 (5 – 33%), 2 (33 – 66%), and 3 (> 66%). Inflammation was scored as 0 (none), 1 (< 2 foci per 200x magnification field), 2 (2 – 4 foci), 3 (> 4 foci). The number of animals with microvesicular/macrovesicular/mixture steatosis is also shown. Figure 4G – J shows representative photomicrographs of H&E-stained liver samples of the different experimental groups: male *Stap1* wild-type (Figure 4G), male *Stap1*$^{-/-}$ (Figure 4H), female *Stap1* wild-type (Figure 4I), female *Stap1*$^{-/-}$ (Figure 4J). The yellow arrow indicated marcovesicular steatosis, and the black arryow microvesicular steatosis. Inflammation is depicted by black arrowhead.

Figure 2B illustrates the abundance of different immune cells in the spleen indicating that in *Stap1*$^{-/-}$ mice there are significant fewer eosinophilic cells ($p < 0.05$), and a non-significant increase in dendritic cells. Supplementary Figure 2C shows the absence of differences in the abundance of different immune cells in blood between the genotypes. The presence of different T cell subsets in spleen, HLN, MLN and blood are presented in Supplementary Figure 3.

Discussion

To investigate the role of STAP1 in cholesterol metabolism, we generated two *Stap1* knockout mouse models. Our results show that loss of STAP1 in both knockout lines does not affect plasma cholesterol levels after chow or a high-fat-high-cholesterol (HFC) diet. Interestingly, HFC-fed *Stap1*$^{-/-}$ mice tended to gain less body weight compared to their wild-type littermates. This combined with a prominent difference in the type of liver steatosis (macrovesicular steatosis in *Stap1*$^{-/-}$ mice and microvesicular steatosis in *Stap1* wild-type mice) in especially male mice provides food for thought how the absence of STAP1 interacts with metabolic pathways.

Conflicting results

Our data are in contrast with earlier findings of hypercholesterolemia in individuals carrying *STAP1* mutations, because STAP1 deficiency in mice does not translate in altered cholesterol phenotype. It is possible that the human mutations may render gain-of-function instead of the anticipated loss-of-function as based on *in silico* predictions. For as far as we know, functional and quantitative measurement of STAP1 levels in individuals carrying mutations have not been performed. We used the CRISPR/Cas9 technology to introduce targeted mutations in *Stap1* exon 3. Exon 3 was preferred because three of the five missense mutations

in humans were found in exon 3. Using transcript specific primers we showed that transcript *Stap1*-201 (*Stap1* transcript without exon 3) was unlikely to be ubiquitously transcribed, therefore *Stap1* exon 3 seemed to be a good target for CRISP/Cas9 genome editing. This was furthermore confirmed by targeted proteomics showing complete absence of STAP1 in knockout mice with a targeted mutation in *Stap1* exon 3. The mouse model used in our analysis mimics a loss-of-function mutation. It should be noted that based on the data presented in this study we cannot exclude that STAP1 overexpression in mice might cause plasma lipid changes. *Stap1* overexpression or knock-in (mimicking human mutations) could for example be used to study this further. It is interesting in this regard that for all major genes involved in familial hypercholesterolemia, both gain- and loss-of-function mutations have been described (*Pcsk9*,[210] *Apob*[211] and *Ldlr*[212, 213]) to affect plasma lipids in mice. With this in mind, our data, which show no plasma lipid phenotype in *Stap1*$^{-/-}$ mice, underline that we should reconsider the role of STAP1 in the control of LDL metabolism.

Another possible explanation for the lack of translation are large differences in cholesterol metabolism between mice and humans. Mice lack cholesteryl ester transfer protein, which facilitates the exchange of cholesteryl esters and triglycerides between HDL and apolipoprotein B (APOB) containing lipoproteins. As a consequence, plasma cholesterol is predominantly carried by HDL particles, whereas in humans LDL particles are the main lipoprotein carrying cholesterol in the blood. Another difference is the alternative RNA editing of *APOB* in humans resulting in APOB48 in the small intestine (on chylomicrons) and APOB100 in the liver (on VLDL) while in mice, only APOB100 is produced at both sites. Another difference in the cholesterol metabolism between mice and humans could be the physiological roles of STAP1. Although we cannot rule this out, the amino acid sequence similarity of STAP1 in mice and humans is higher than 80% and in both species the protein encompasses the PH and SRC 2 domains. On the other hand, *STAP1* encodes for one protein-coding transcript in humans, but the *Stap1* gene in mice for two of which one lacks the exon in which most human mutations were identified. However, mutations introduced in *Stap1* exon 3 leads to a complete deficiency of STAP1 in mice.

Evaluation of human data

Thus far, two different research groups have shown associations between *STAP1* variants and FH.[205, 206] It is in the context of the current findings possible that these mutations do not change *STAP1* function but are mere chance findings. The original linkage analysis study may e.g. have suffered from incorrect assignment of affected and unaffected individuals due to overlapping LDL-c values in both groups. When critically reviewing the genetic and phenotypic evidence of *STAP1* mutations it becomes also clear that the phenotype of patients with *STAP1* mutations is relatively mild compared to *LDLR* and *APOB* mutation carriers, and the penetrance is incomplete. Beyond the discovery of *STAP1* mutations in

families with hypercholesterolemia, the largest GWAS conducted thus far have not picked up variants located in the *STAP1* locus (enlarged to 1Mb) that are associated with total cholesterol and LDL-c traits.[214, 215] Unfortunately, *STAP1* mutations were not found in the context of hypercholesterolemia by the UK10K Consortium,[216] neither in the Copenhagen City Heart Study (in 100 individuals with the most extreme LDL cholesterol for age and gender; personal communication A. Tybjaerg Hanssen), nor in the LIPIGEN study (1,592 individuals with clinical diagnosis of definite or probable FH),[217] and neither in 103 patients with premature acute coronary syndrome and LDL-c ≥ 4.1 mmol/l.[218] Taken together, the genetic evidence that *STAP1* is playing a role in lipid metabolism is rather weak.

Although there is currently only scarce evidence of STAP1 playing a role in cholesterol metabolism, there are several indications that it may actually play a role in triglyceride metabolism. The first carriers of *STAP1* mutations, studied by Fouchier et al[205] presented with significantly higher triglyceride levels, compared to *LDLR* and *APOB* mutation carriers. In line, *STAP1* gene expression in leukocytes was recently shown to be positively correlated with plasma triglyceride levels.[219] In our study, we did not observe significant changes in triglyceride levels between *Stap1* genotypes, however female *Stap1*$^{-/-}$ mice tended to have lower triglyceride levels in comparison to wild-type littermates. These findings combined warrant further investigation into this direction.

STAP1 and body weight

The present study was not set up to explore the pronounced reduced body weight gain when fed with HFC-diet in *Stap1*$^{-/-}$ male mice. The mechanisms underlying the control of body weight are known to be complex and simultaneously not completely explored. In mice, changes in body weight are a consequence of for example differences in metabolic pathways (e.g. resting metabolic rate), energy expenditure, food intake (or uptake in the gastrointestinal tract), or gut microbiota. However, the difference in body weight might not warrant further investigation because Reed et al showed that of 1,977 knockout mouse strains, 31% presented with lower body weight.[220]

STAP1 and immune system

Our initial disappointing results concerning plasma cholesterol levels, have forced us to rethink how STAP1 expression in mainly cells of the immune system may affect plasma lipids. Our protein analyses confirm that in mice, STAP1 is present in the thymus and spleen, underling a role in the immune system. [207, 208] It remains possible that attenuated or enhanced STAP1 function affects receptor tyrosine kinases, especially c-kit. It is in this regard of interest to note that gain-of-function mutations in c-kit cause leukemia,[221] and leukemia in turn are associated with hypocholesterolemia.[222] In addition, administration of tyrosine

kinase inhibitors can cause hypercholesterolemia in patients with leukemia.[223] So far, we have hardly addressed possible changes in the immune system of the *Stap1*$^{-/-}$ mice and ongoing studies will hopefully provide clues towards association of the observed metabolic phenotype including an effect on triglycerides that we observed in our female mice.

Interestingly, pharmaceutical interventions targeting inflammation in the prevention of CVD are on the rise.[224] Perhaps STAP1 intervention could also play a role in the progression of atherosclerosis.

Conclusions

Taken together, a complete loss of *Stap1* in mice does not affect plasma cholesterol levels but has interesting effects on body weight gain and hepatic steatosis when fed a high-fat-high-cholesterol diet. Further studies into the effect of *Stap1* deficiency on the immune system are ongoing.

Supplementary material

Supplementary Table 1. Stain 1.

Antigen	Label
Dead/live	APC-Cy7
CD19	PeCy7
B220	BV500
CD21	BV421
CD23	PE
CD93	PerCP-Cy 5.5
IgD	APC
IgM	FITC

Supplementary Table 2. Stain 2.

Antigen	Label
Dead/live	APC-Cy7
B220	FITC
NK1.1	FITC
CD11b	eFluor450
Ly6G	PE
CD11c	APC
Ly6C	PerCP-Cy5.5

Supplementary Table 3. Stain 3.

Antigen	Label
Dead/Live	APC-Cy7
CD8	eFluor 450
CD4	PerCP
CD44	APC
CD62l	FITC
CD25	PE

Supplementary Table 4. Differentiation of cell subsets using markers.

	B220/NK1.1	CD11b	Ly6G	Ly6C	CD11c
Neutrophils	-	+	+	-	-
Eosinophils	-	+	-	-	-
Monocytes	-	+	-	+/-	-
Inflammatory monocytes	-	+	-	+	-
Non-inflammatory monocytes	-	+	-	-	-
	CD8	**CD4**	**CD62l**	**CD44**	**CD25**
CD8 T cells	+	n/a	n/a	n/a	n/a
CD4 T cells	n/a	+	n/a	n/a	n/a
Naive T cells	n/a	+	+	-	n/a
Effector T cells	n/a	+	-	+	n/a
Regulatory T cells	-	+	-	-	+

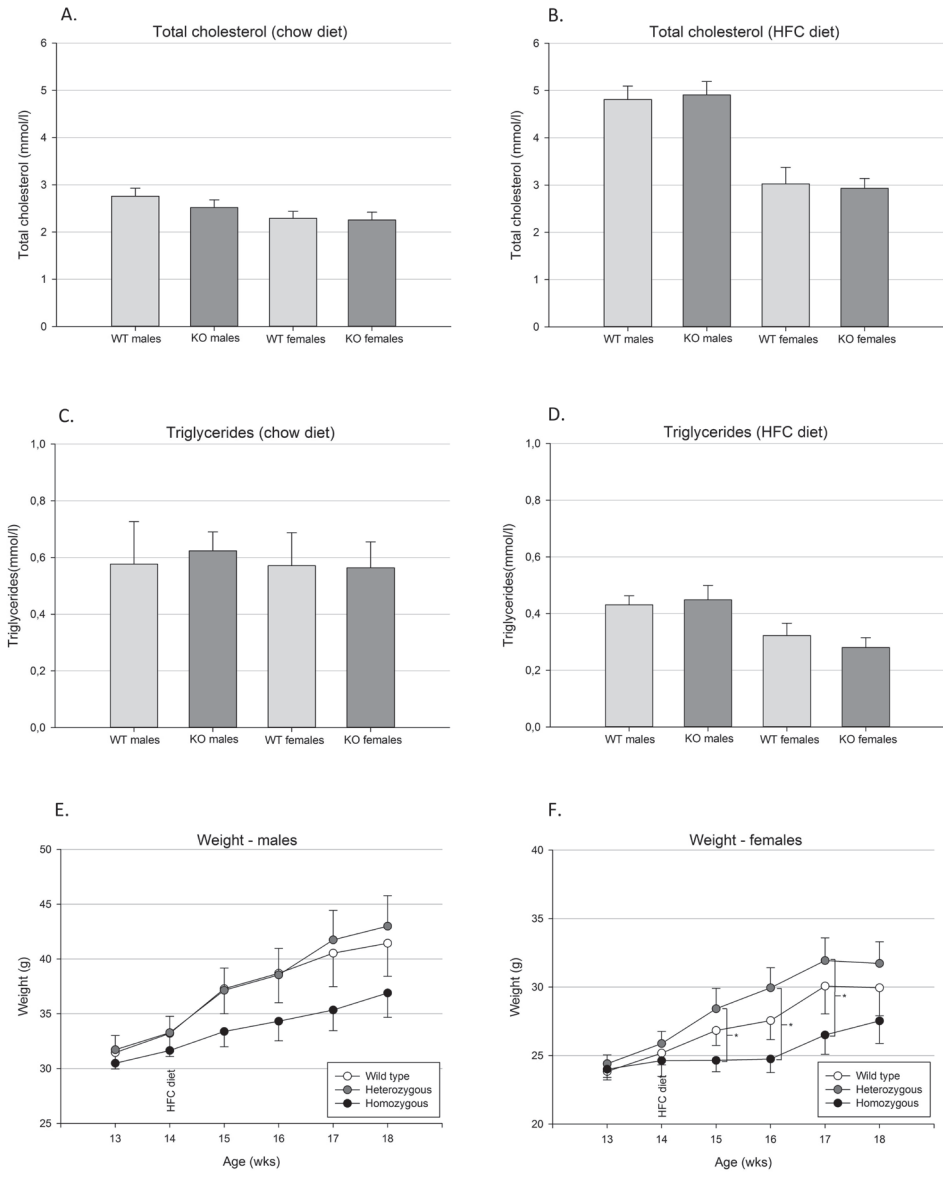

Supplementary Figure 1. Characterization Stap1$^{-/-}$ mice with del14nt. No differences were present between the genotypes in plasma lipids levels (Figure S1A – S1D). The weight of the mice are shown in Figure S1E for males and S1F for females. In both males as females the *Stap1*$^{-/-}$ mice gained less weight during the HFC-diet intervention. This was significant in the females.

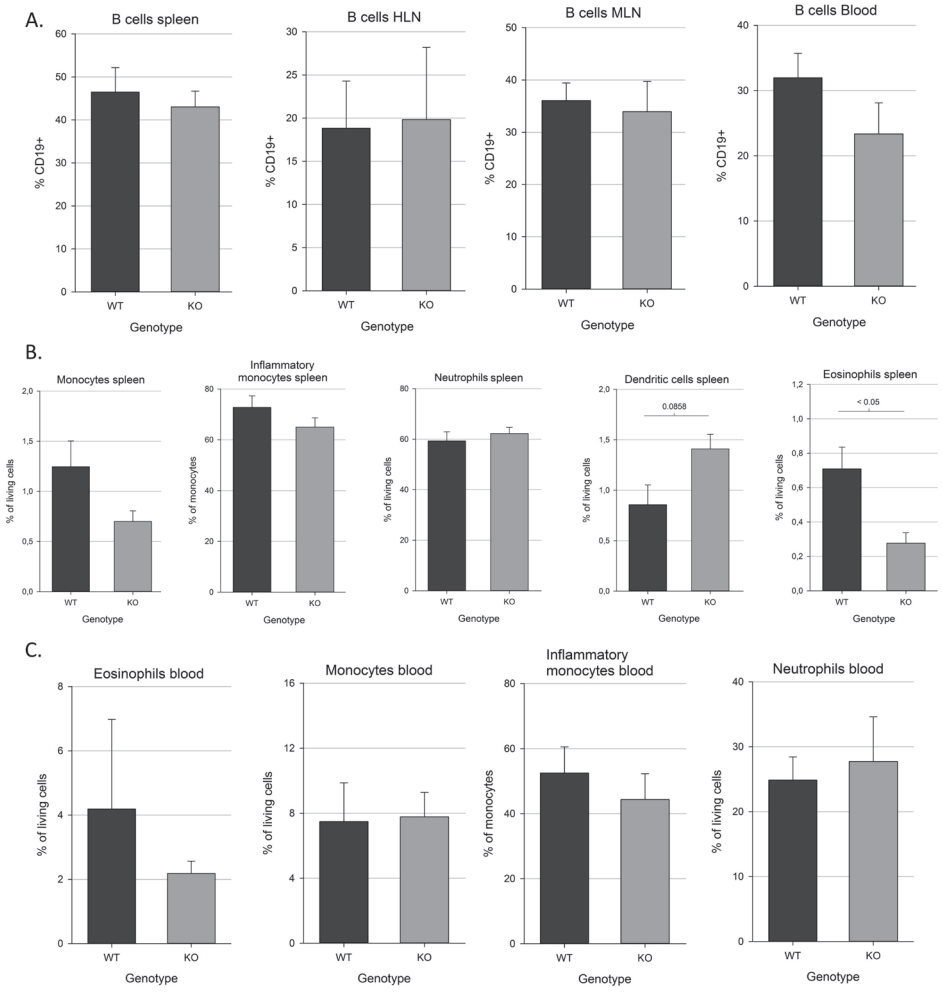

Supplementary Figure 2. Flow cytometry analysis. Flow cytometry analyses were performed on the harvested tissues of three *Stap1*$^{-/-}$ mice and three wild-type littermates. Data are presented as mean and standard deviation. Significant differences (p-value < 0.05) between genotypes are marked with an asterisk. Panel A: the number of B cells in different tissues. Panel B: different immune cell subsets in the spleen. Panel C: the presence of several immune cells in blood.
Abbreviations: HLN, heart lymph nodes; MLN, mesenteric lymph nodes.

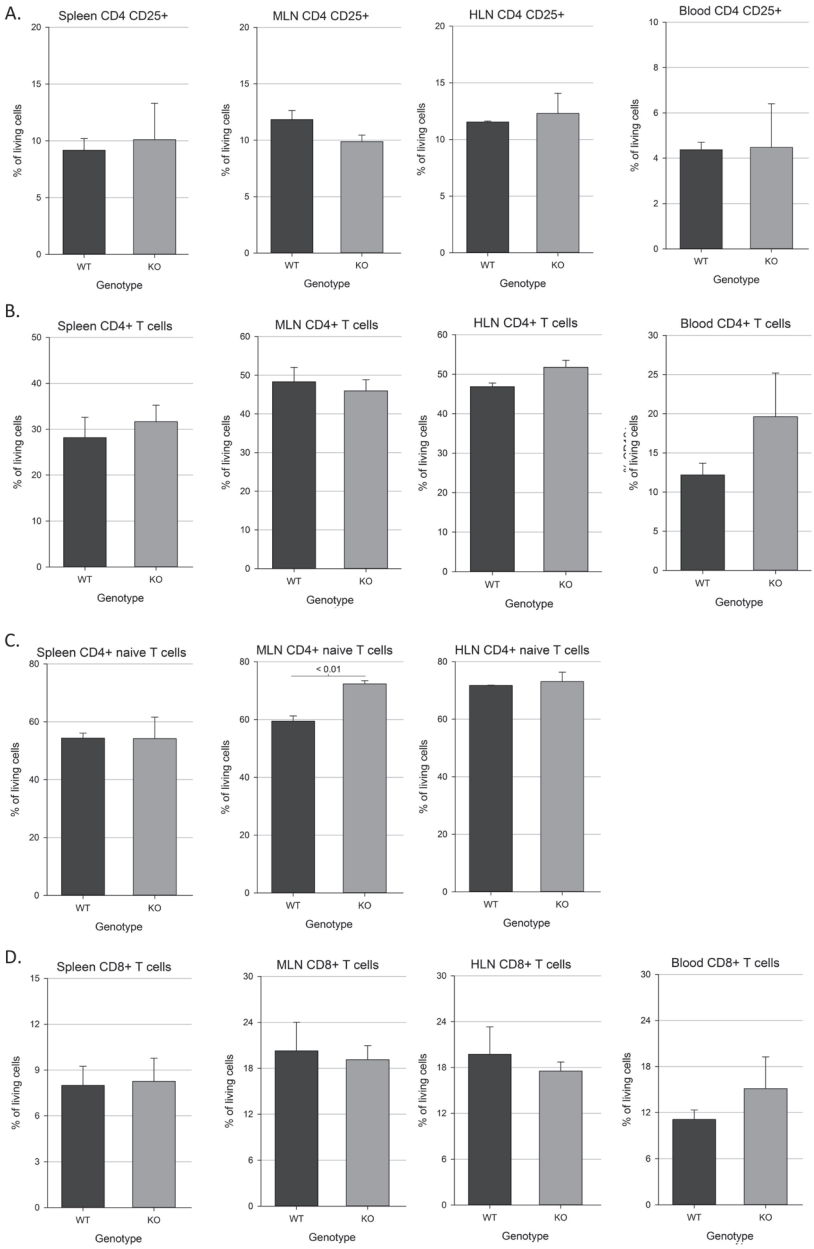

Supplementary Figure 3. Flow cytometry analysis. Flow cytometry analyses were performed on the harvested tissues of three *Stap1*$^{-/-}$ mice and three wild-type littermates. Data are presented as mean and standard deviation. Significant differences (p-value < 0.05) between genotypes are marked with an asterisk. The number of CD4 CD25+ cells (Panel A), CD 4 T cells (Panel B), CD 4 naïve T cells (Panel C) and CD 8 T-cells (Panel D) for different tissues are presented.

Abbreviations: HLN, heart lymph nodes; MLN, mesenteric lymph nodes.